Interdecadal variability of the summer precipitation in China and its possible cause

Ding Yihui, Sun Ying and Wang Zunya
National Climate Center,
China Meteorological Administration,
Beijing 100081

Outline

1. Interdecadal regime shift of the summer precipitation in East China
2. Associated interdecadal variability of large-scale circulation features in the Asian monsoon region
3. Possible causes
4. Projection of the next regime shift of precipitation in China

(a) North China

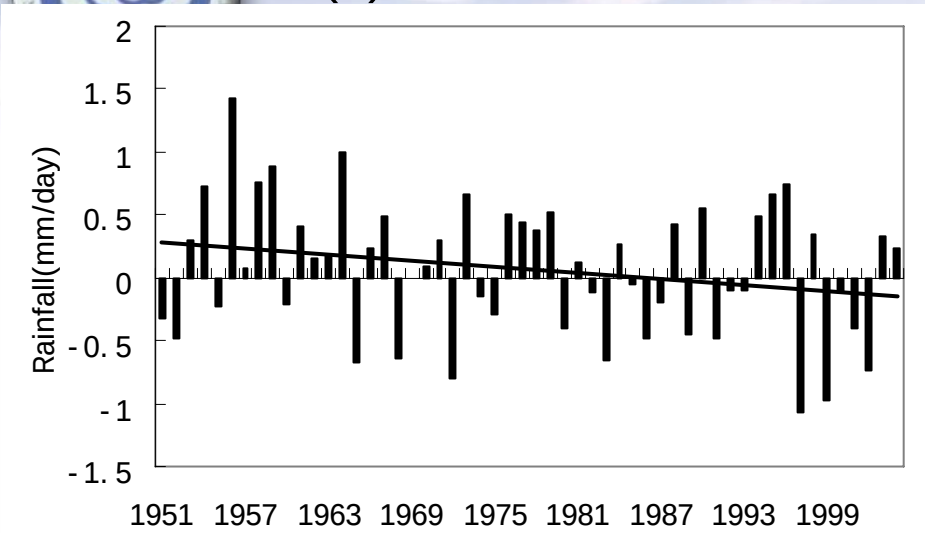

(b) The Yangtze River valley

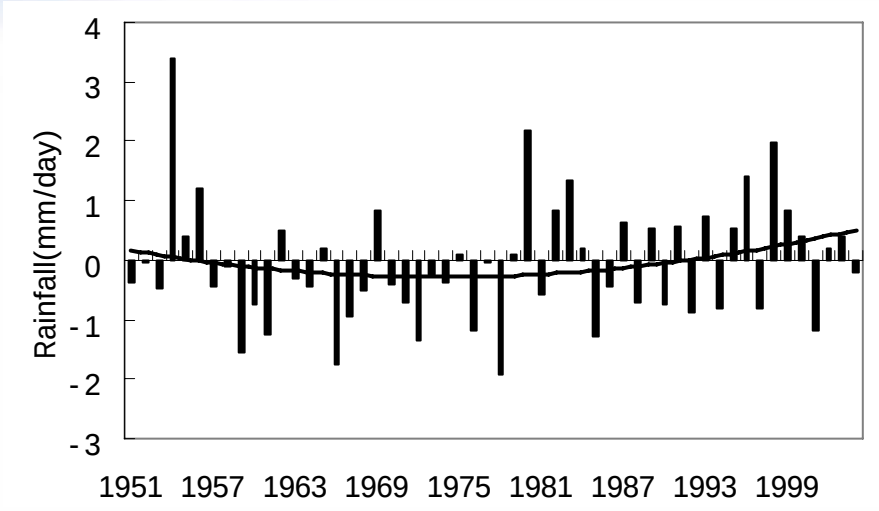

(c) South China

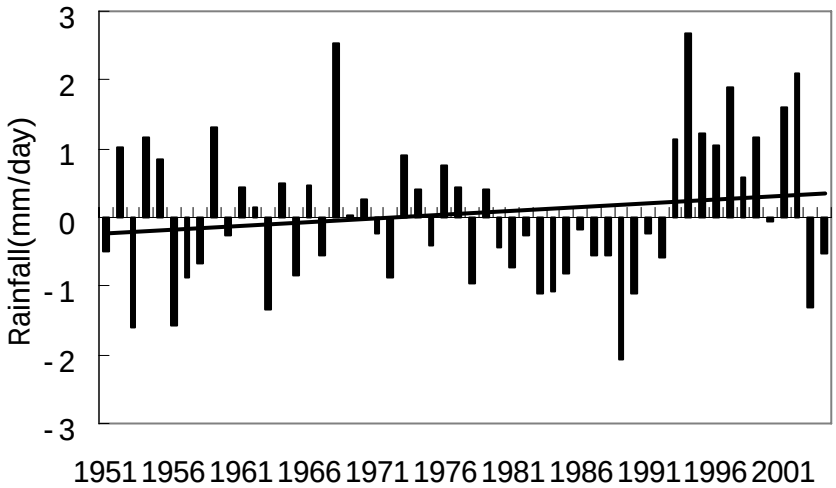

Figure 1 Time series of summer (June, July and August) precipitation departures from climatological mean (1971-2000) for North China (107.5-120° E, 34-43° N) (a), the Central China (the Yangtze River Basin:107-122° E, 28-34° N(b) and South China (107.5-122° E, 22-28° N) (c). Bold lines denote linear trends. Unit: mm day^{-1}

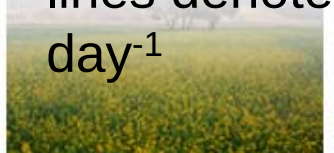

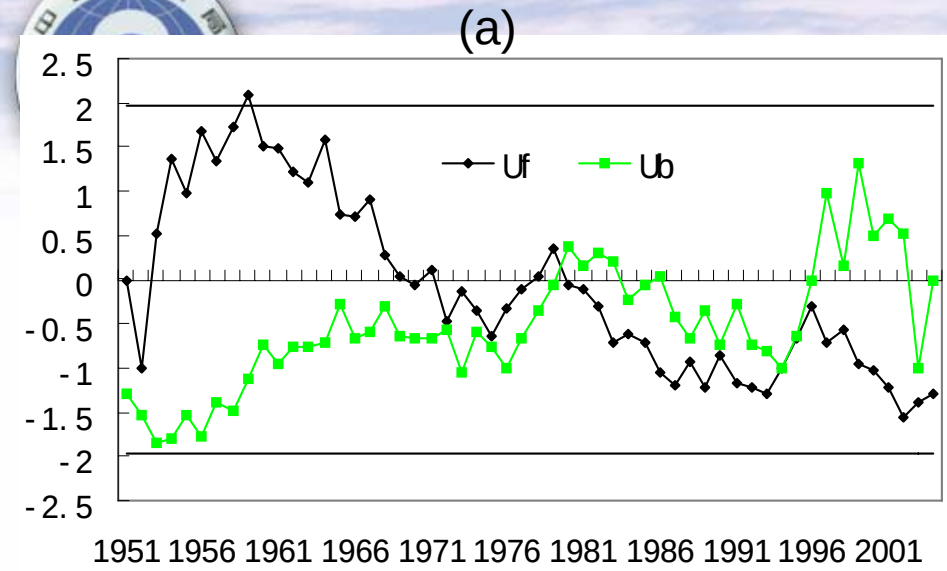

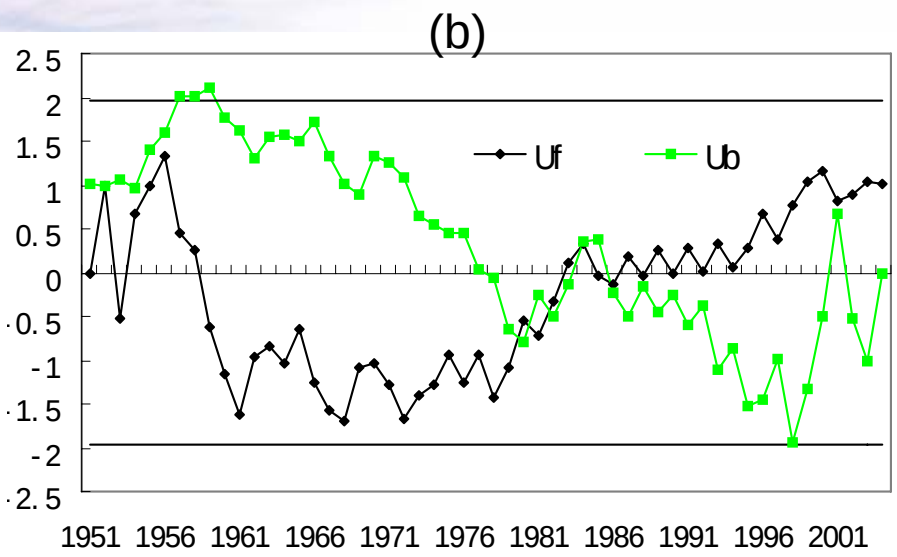

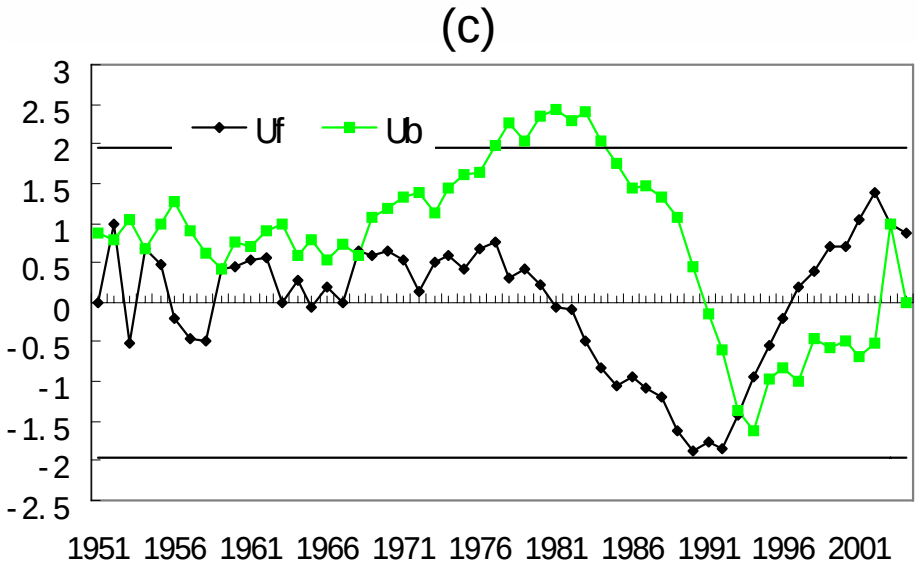

Figure 2 Tests of summer precipitation trends by using M-K method for North China (a), the central China (b) and South China (c).

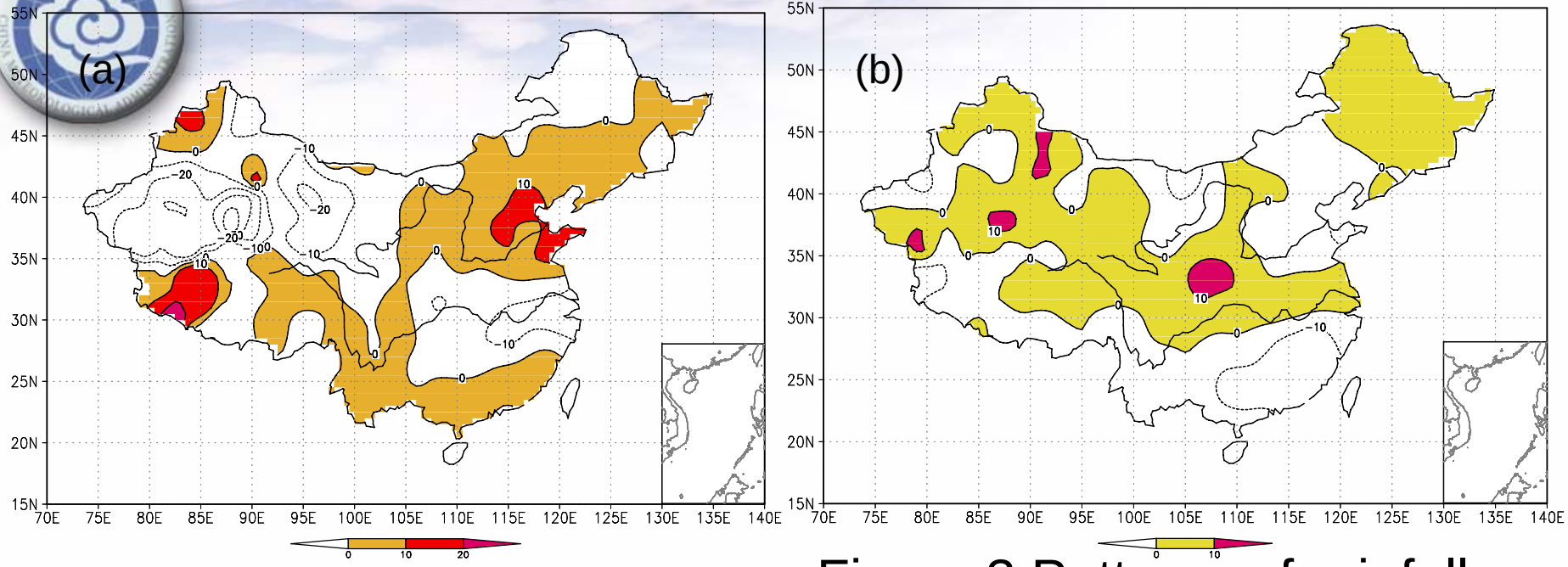

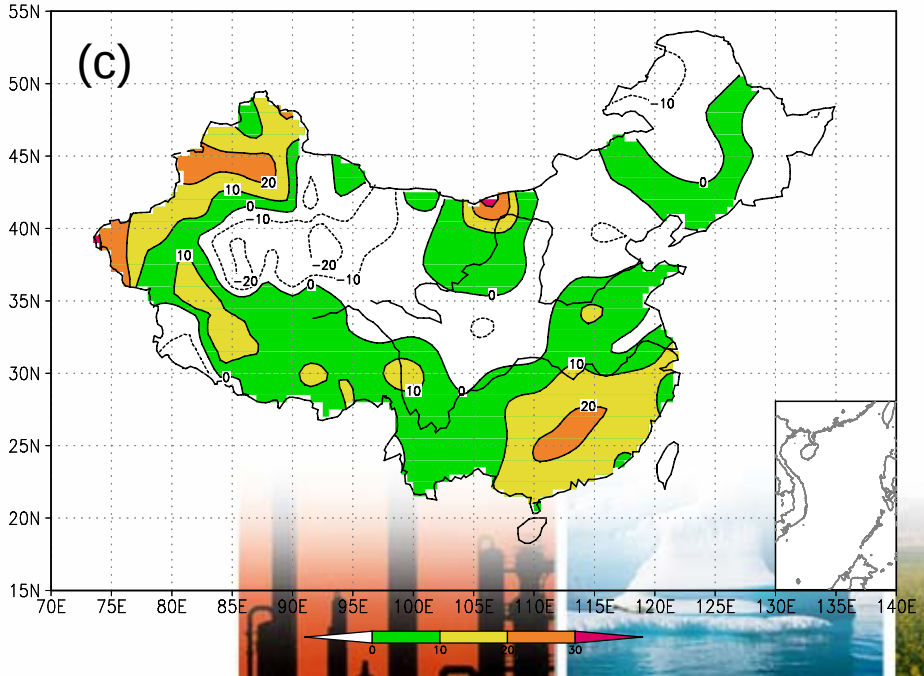

Figure 3 Patterns of rainfall departure percentage for summer (JJA) (%) averaged for 1951-1978 (a), for 1979-1992 (b) and for 1993-2004 (c). Departures are relative to the climatological mean of 1971-2000 based on 704 surface station in China

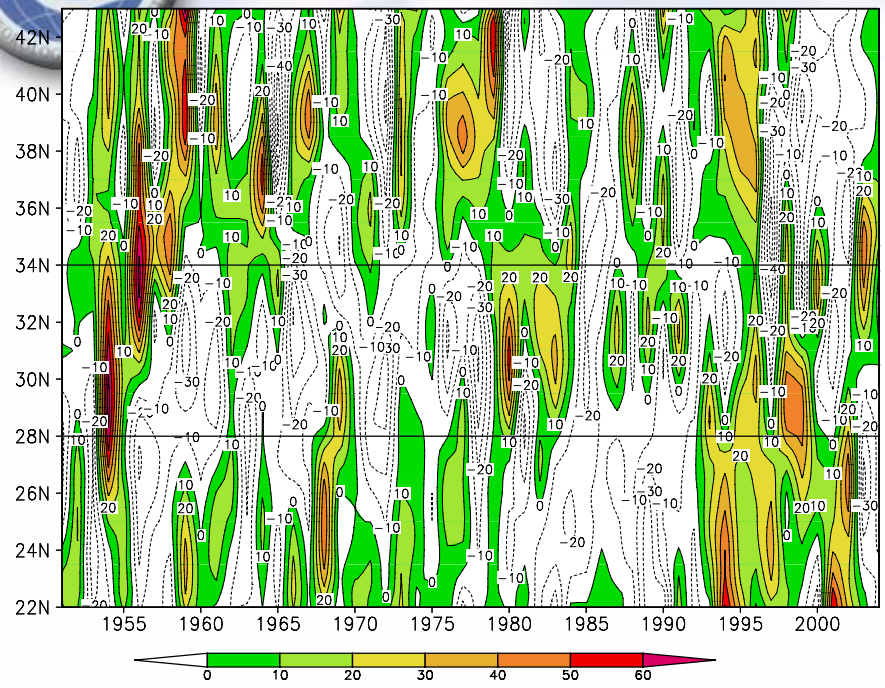

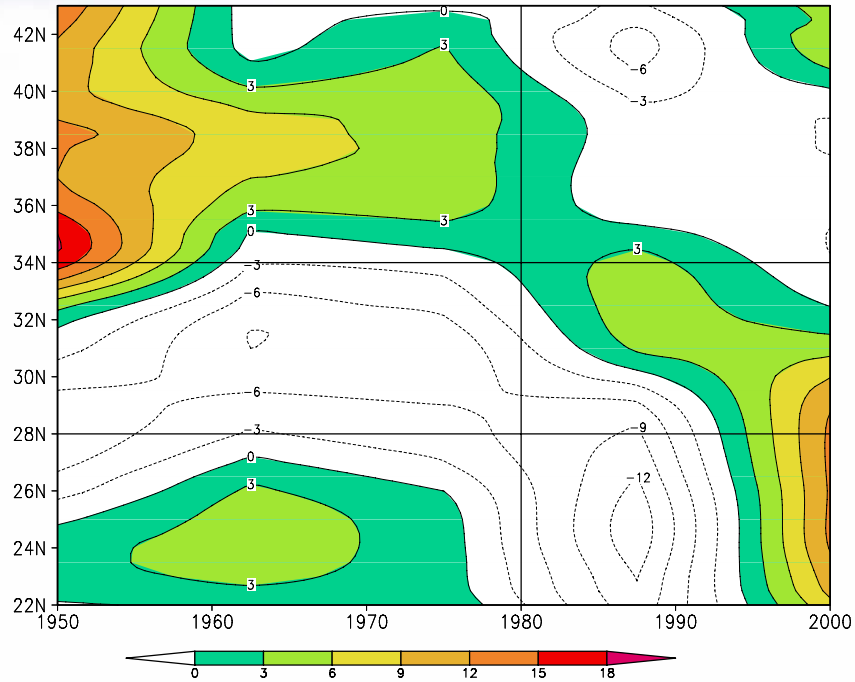

Figure 4 Latitude-time cross-sections of the anomalous precipitation in summer of 1951-2004 for East China (105-120° E) (a) and the 10-yr running precipitation (b). Unit: mm

2. Associated interdecadal variability of large-scale circulation features in the Asian monsoon region

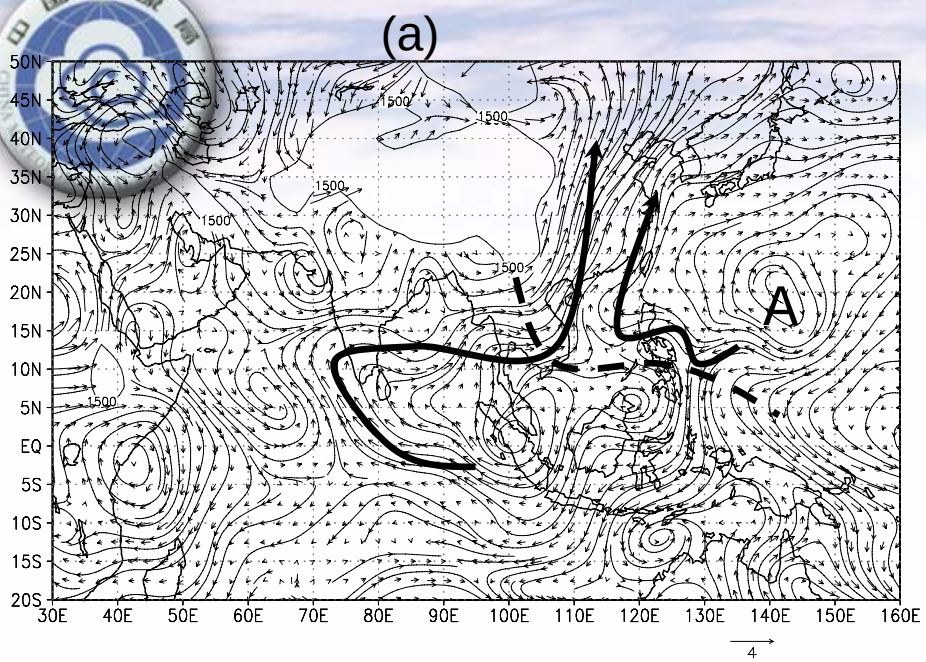

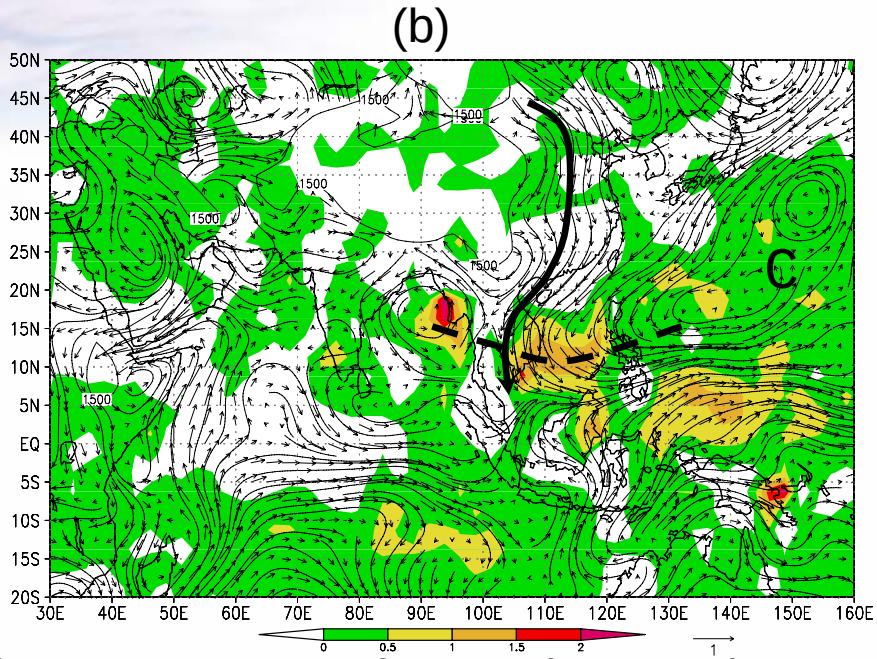

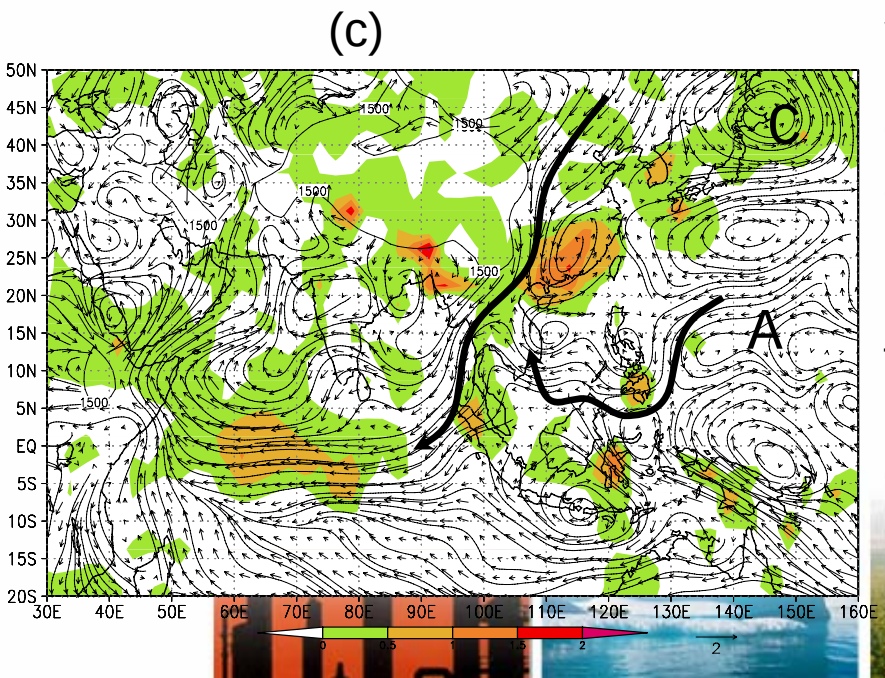

Figure 5 Patterns of anomalous 850hPa stream lines (Unit: m/s) and precipitation (Unit: mm/day) in summer relative to the climatological JJA mean of 1971-2000 averaged for 1951-1978 (a), for 1979-1992 (b) and for 1993-2004 (c). The Xie-Arkin precipitation dataset was used for (b) (c), but for (a), it is not available. Letters A and C represent anomalous anticyclonic and cyclonic circulation systems. Shaded areas denote precipitation anomalies and the configuration of the Tibetan Plateau is depicted with 1500m evevlation isoline.

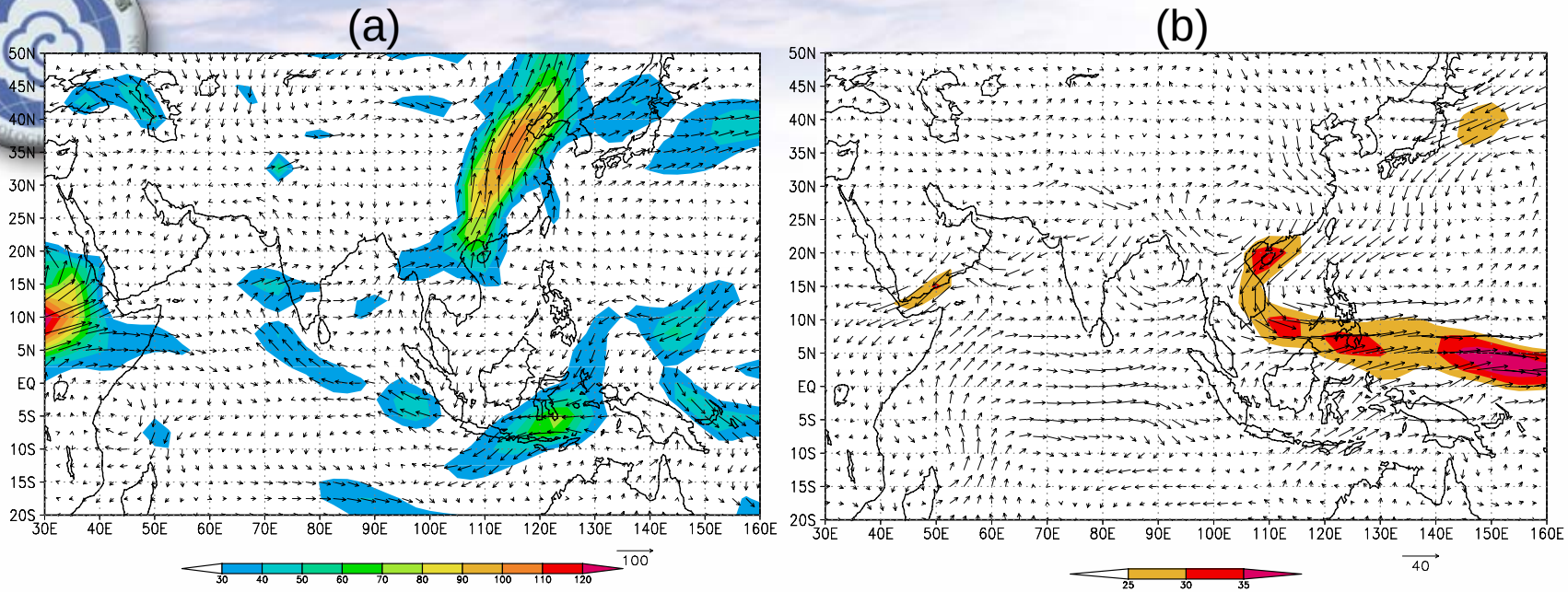

Figure 6 Patterns of anomalous vertically integrated moisture transport (surfact-300hPa) in summer averaged for 1951-1978 (a), for 1979-1992 (b) and for 1993-2004 (c). Unit: $Kgm^{-1}s^{-1}$. Shaded areas denote strong moisture transport.

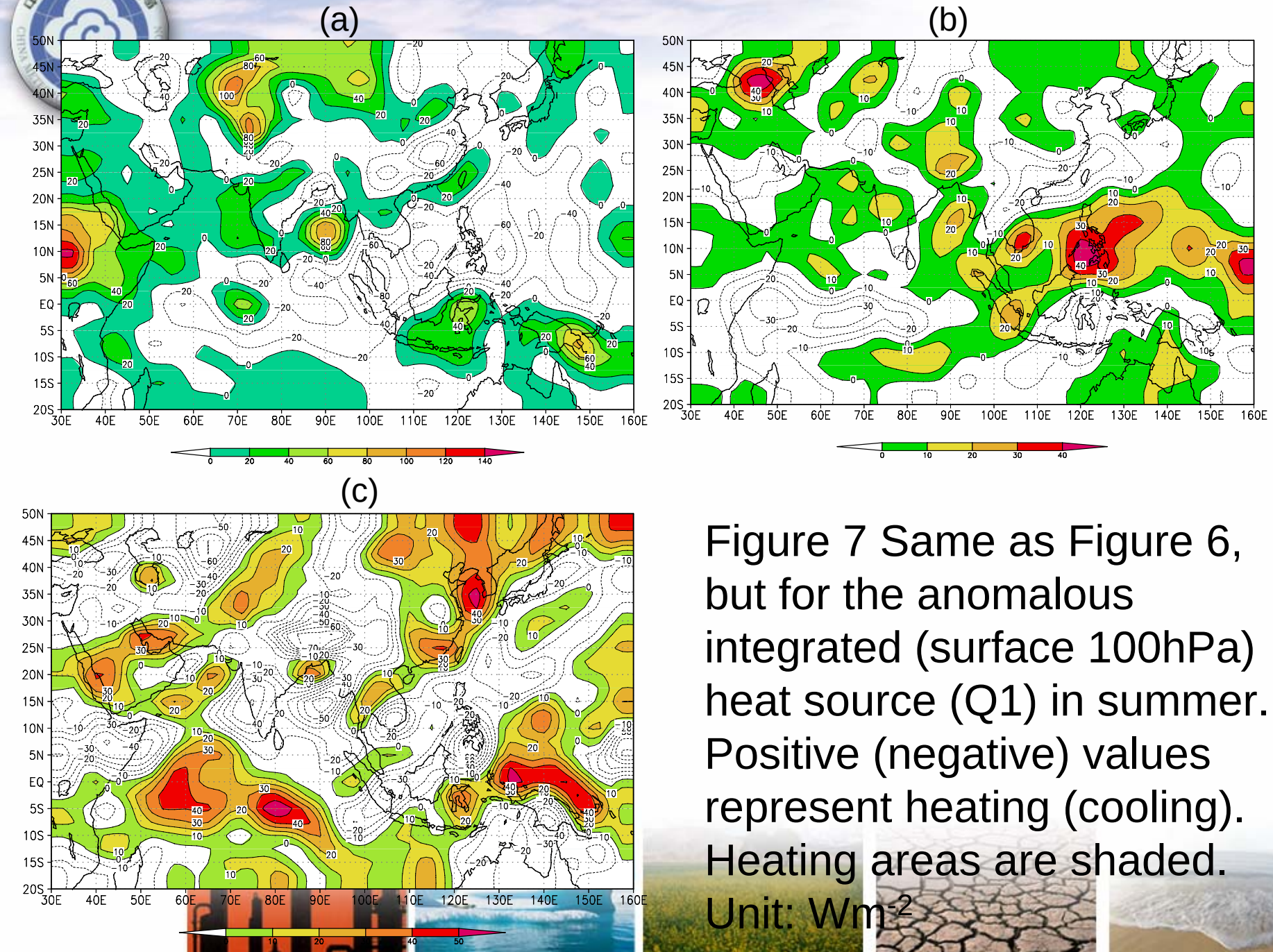

Figure 7 Same as Figure 6, but for the anomalous integrated (surface 100hPa) heat source (Q1) in summer. Positive (negative) values represent heating (cooling). Heating areas are shaded. Unit: Wm^{-2}

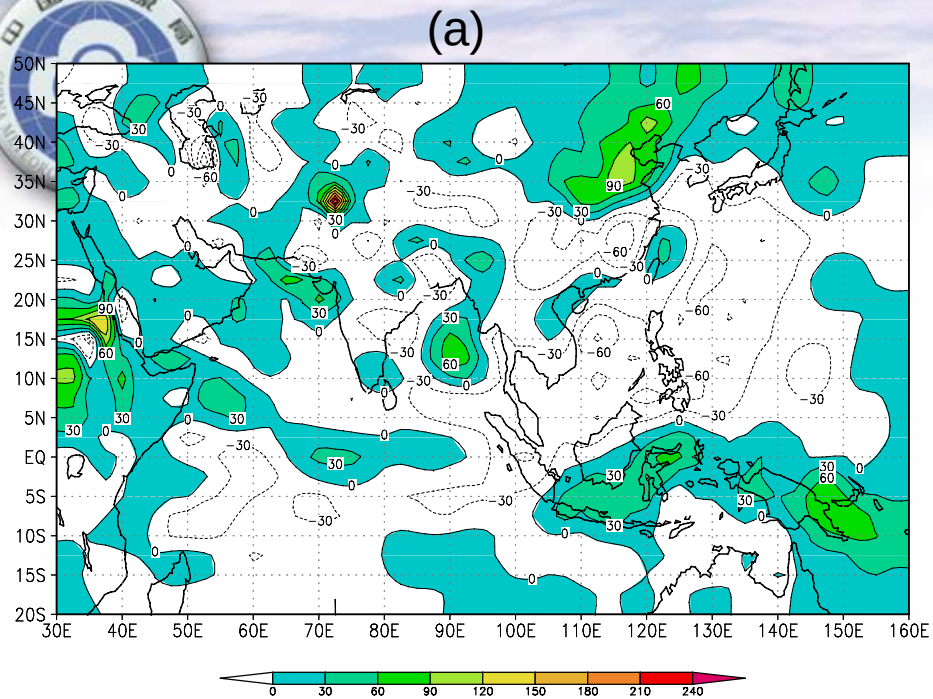

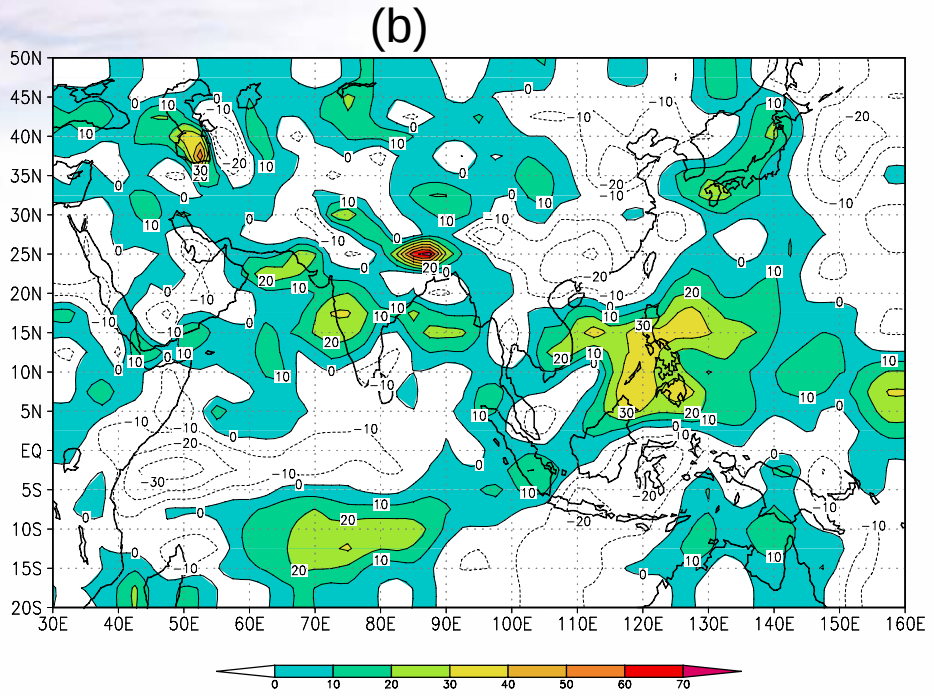

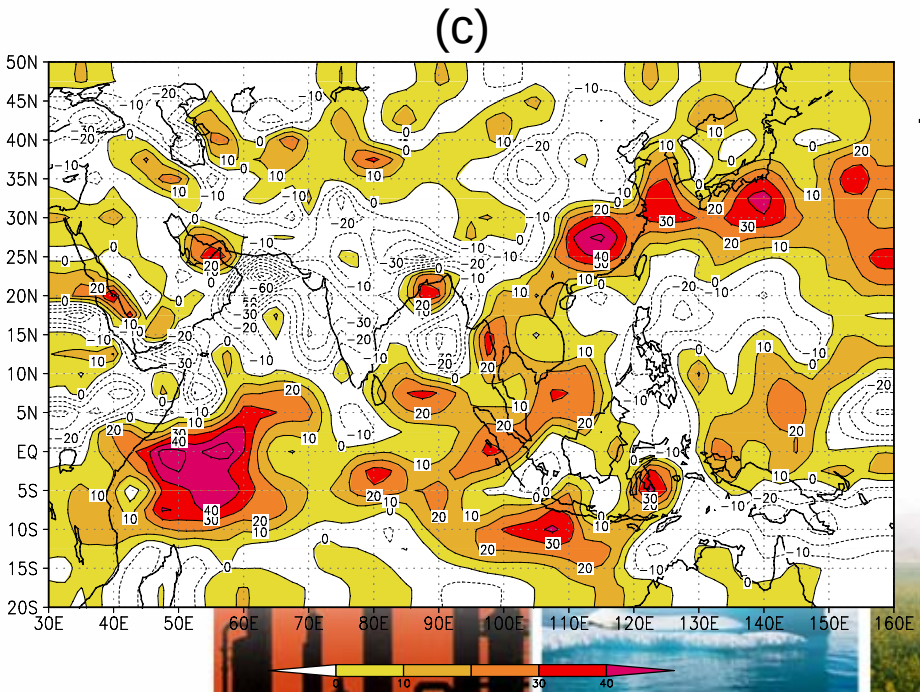

Figure 8 Same as Figure 6,but for anomalous vertically integrated moisture sink (Q2). Pasitive (negative) values represent moisture convergence (divergence). Unit: 10^{-5} $Kgm^{-2}s^{-1}$. Moisture convergence areas are shaded.

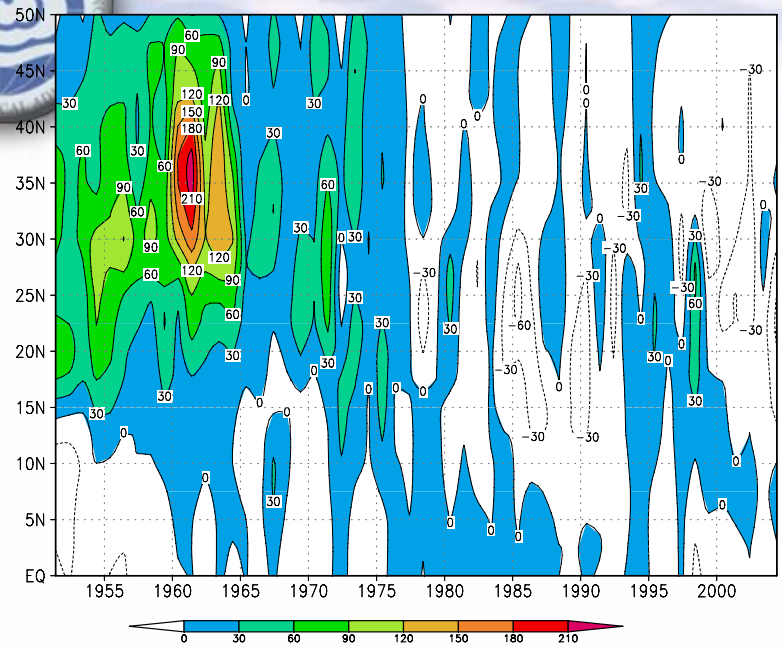

(a)

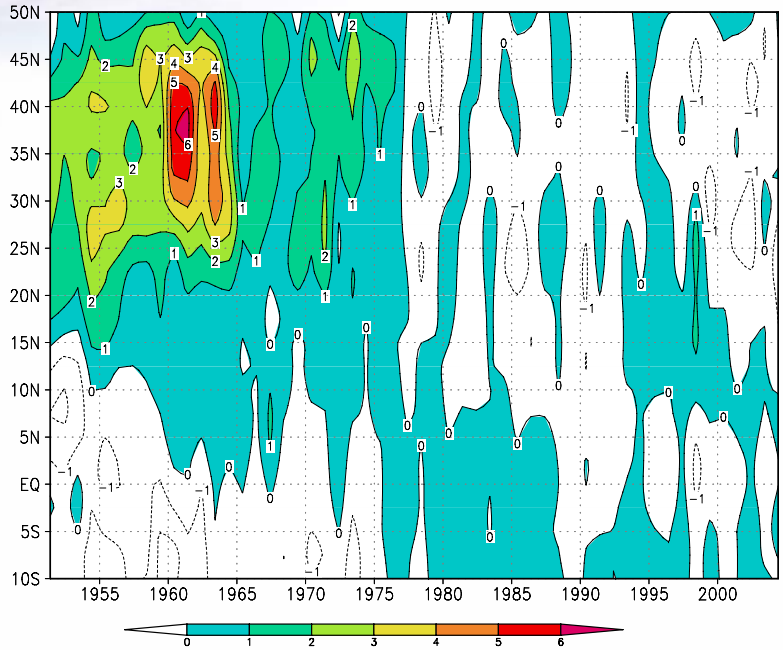

(b)

Figure 9 Latitude-time cross-sections of anomalous vertically integrated (surface-300hPa) moisture transport in summer for 1995-2004 (a) and the moisture sink (Q2) (b). Northward transport and moisture convergence (positive Q2) are shaded. Unit: $Kgm^{-1}g^{-1}$for (a) and $10^{-5}Kgm^{-1}s^{-1}$ for (b).

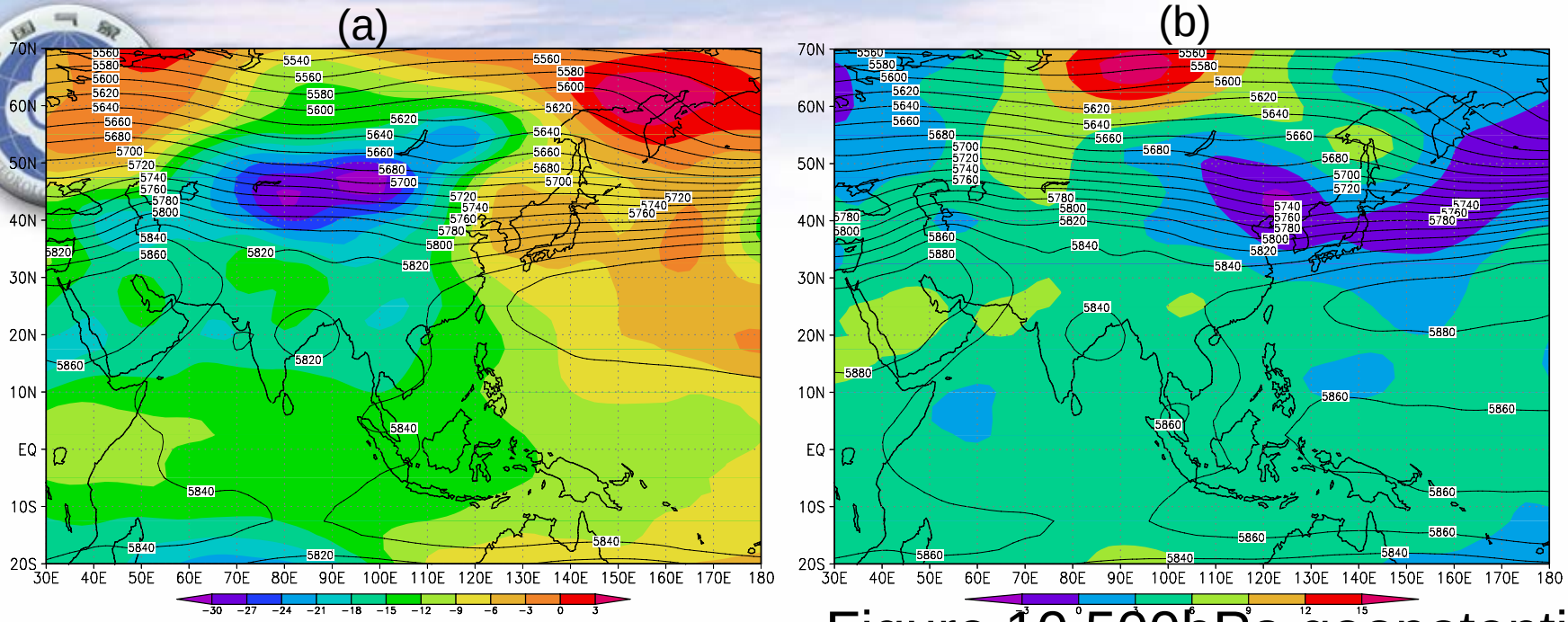

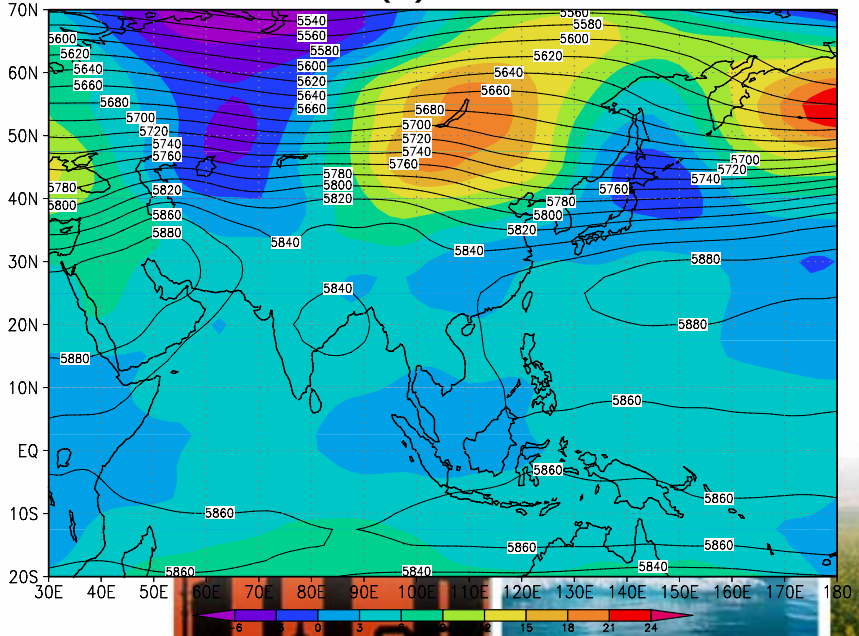

Figure 10 500hPa geopotential height fields in summer, averaged for 1951-1978 (a), for 1979-1992 (b) and for 1993-2004 (c). Unit: gpm. The height anomaly is indicated with colour scale. Latters H and L denote positive and negative anomolous height centers, respectively. Unit: 10gpm.

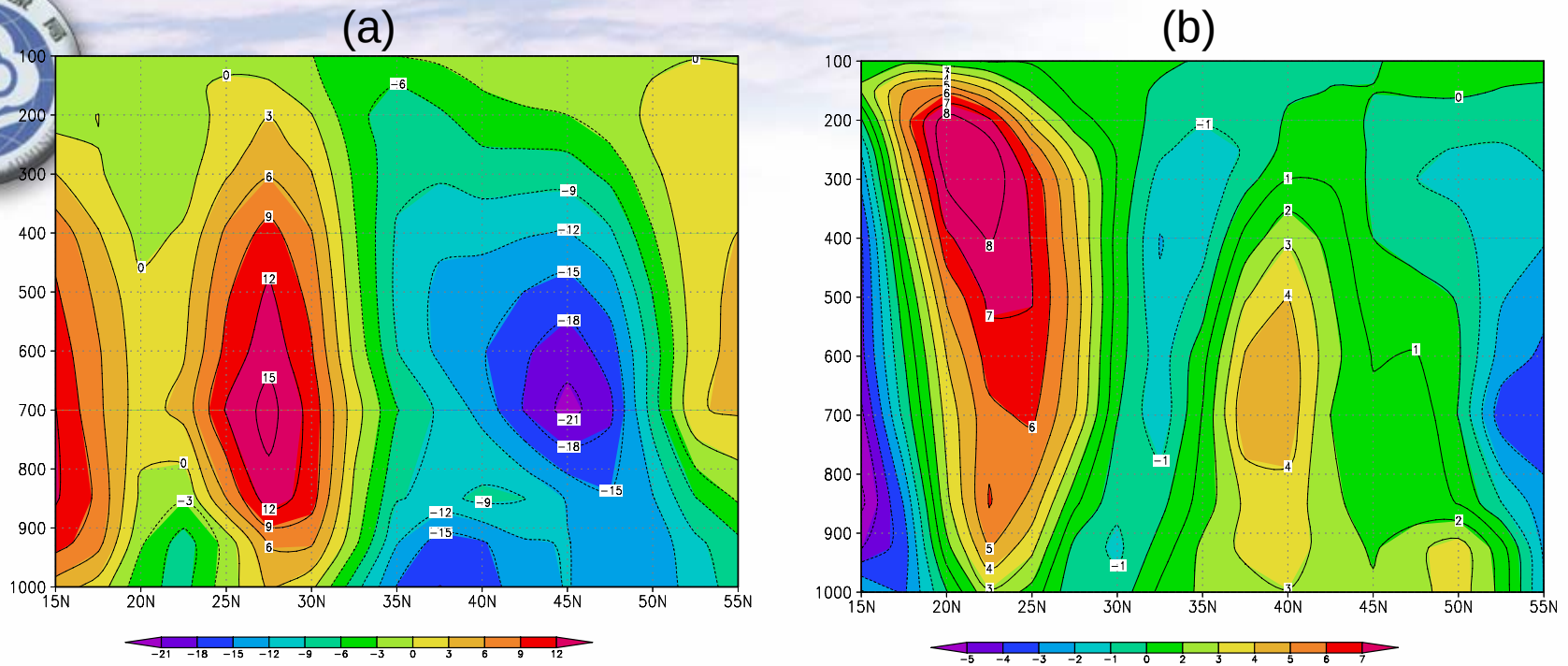

Figure 11 Latitude-time cross-sections of the anomalous vertical velocity ($\omega = dp/dt$) in summer averaged for 1951-1978 (a), for 1979-1992 and for 1993-2004 (c). Unit: 10^{-3} hPas^{-1}

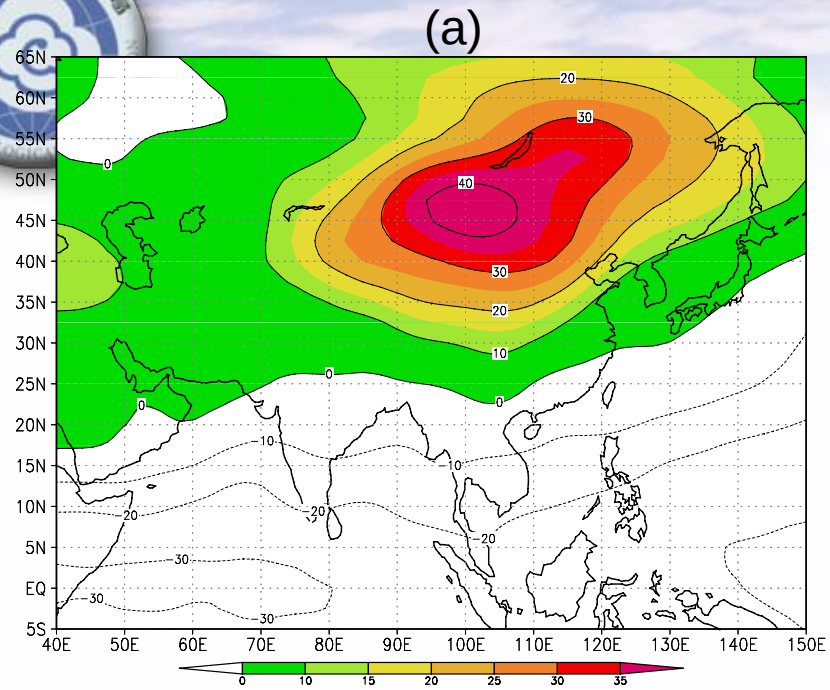

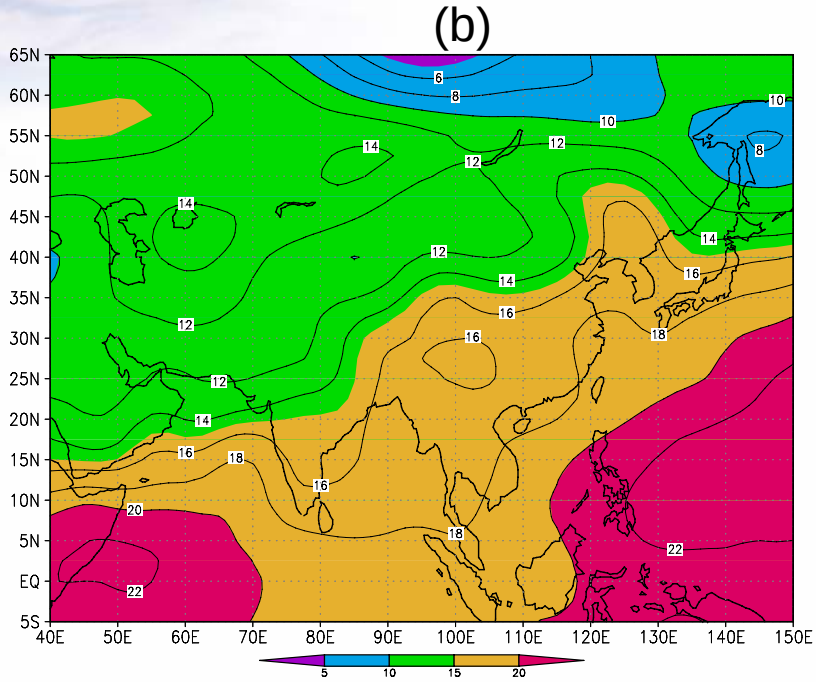

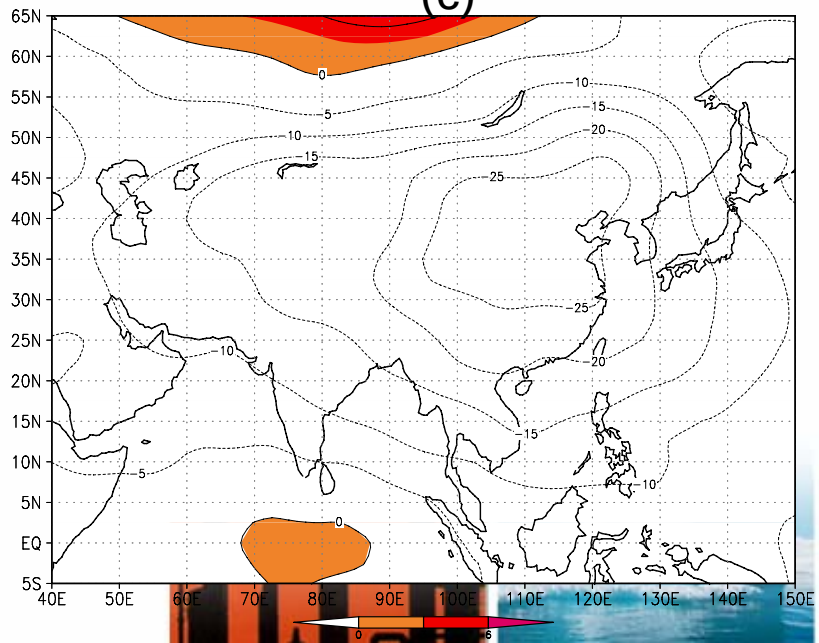

Figure 12 Patterns of the anomalous thickness between 100hPa and 500hPa geopotential height in summer averaged for 1951-1978 (a), for 1979-1992 (b) and for 1991-2004 (c). The climatological mean of 1971-2000 is used. Unit: gpm

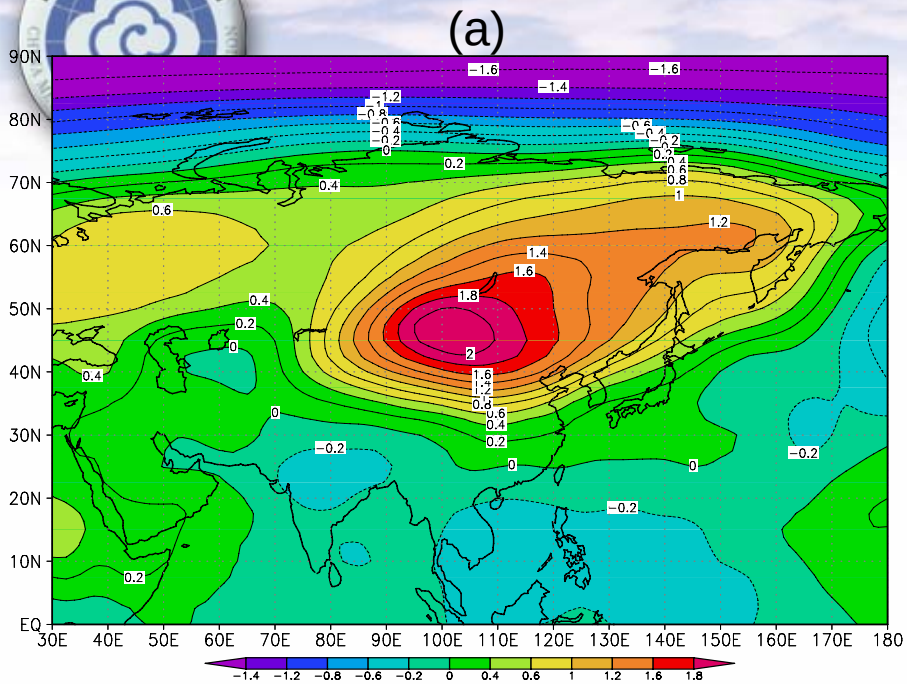

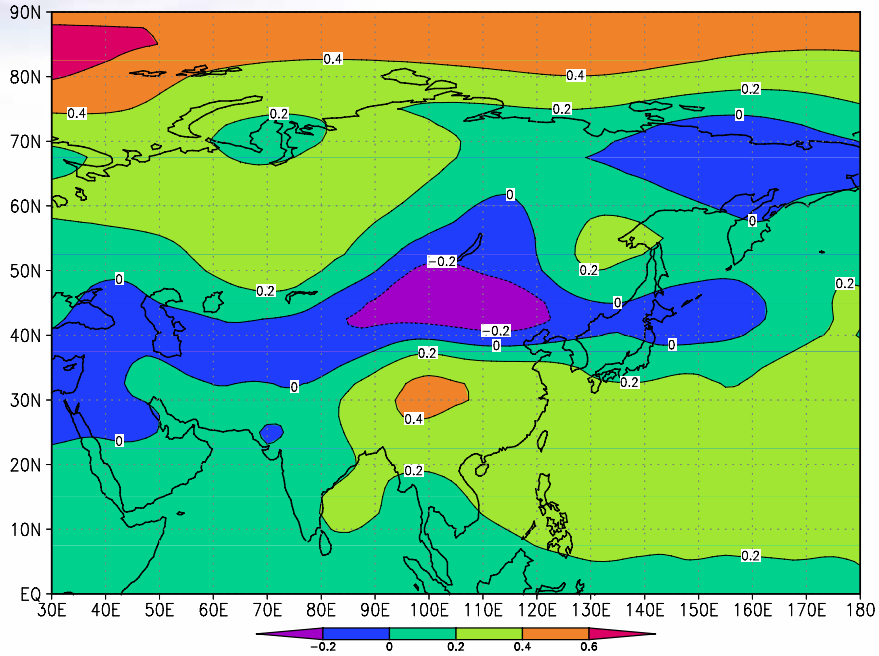

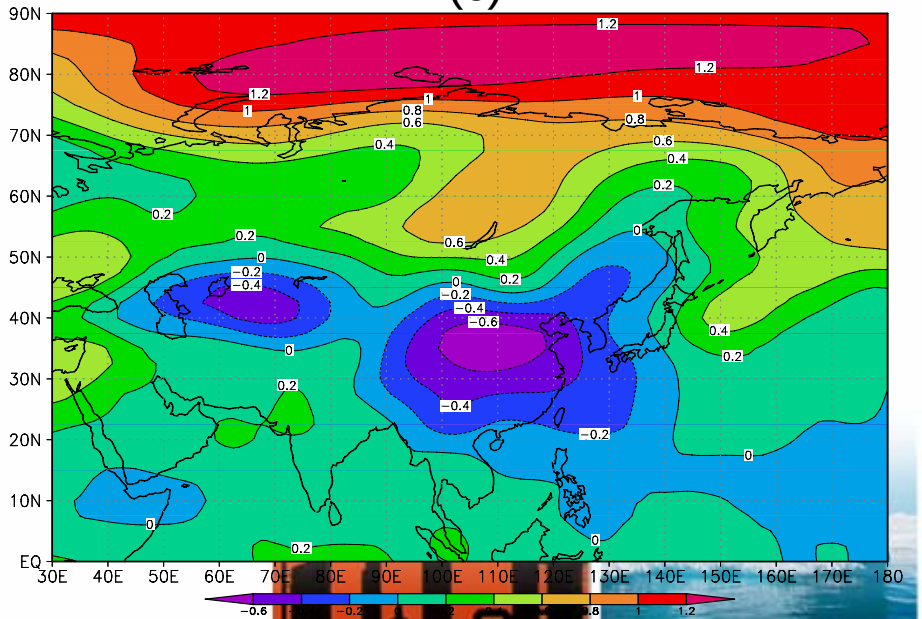

Figure 13 Same as Figure 12, but for 300hPa anomalous temperature in summer. Unit: ℃

3. Possible cause

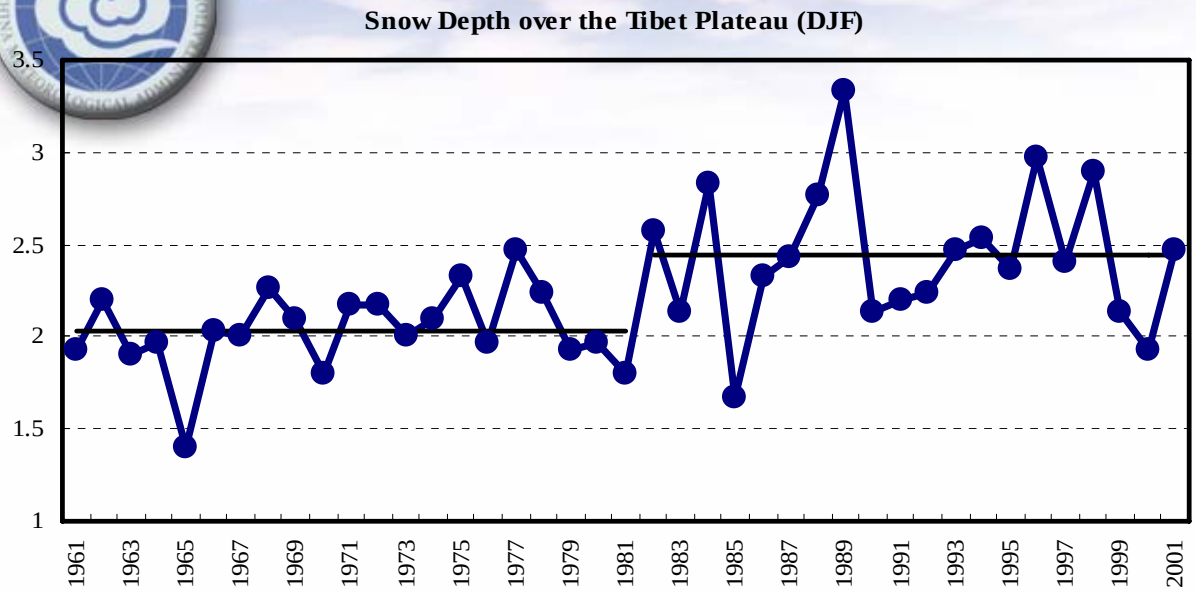

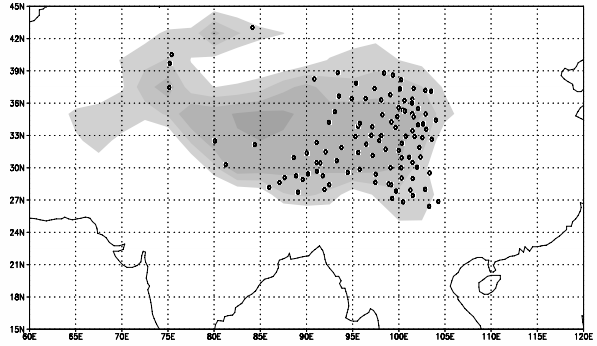

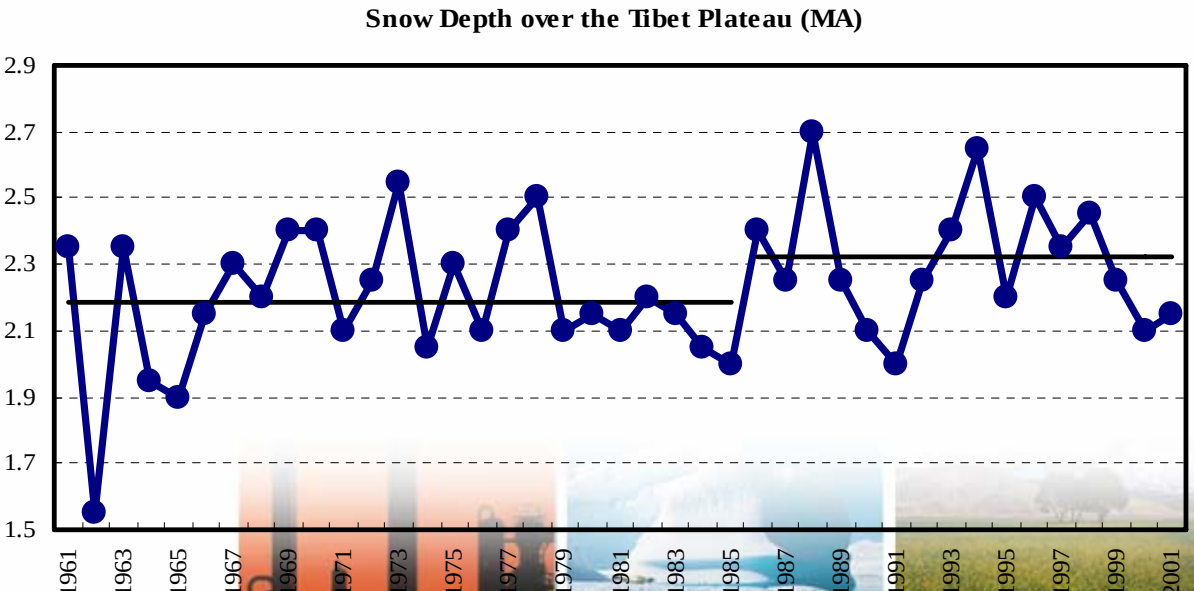

Figure 14 Time-series of snow depth over the Tibetan Plateau averaged for 62 surface stations for winter (December, January and February) (a) and for spring (March and April) (b). Horizontal bars represent averages for different periods. Unit: mm.

(a)

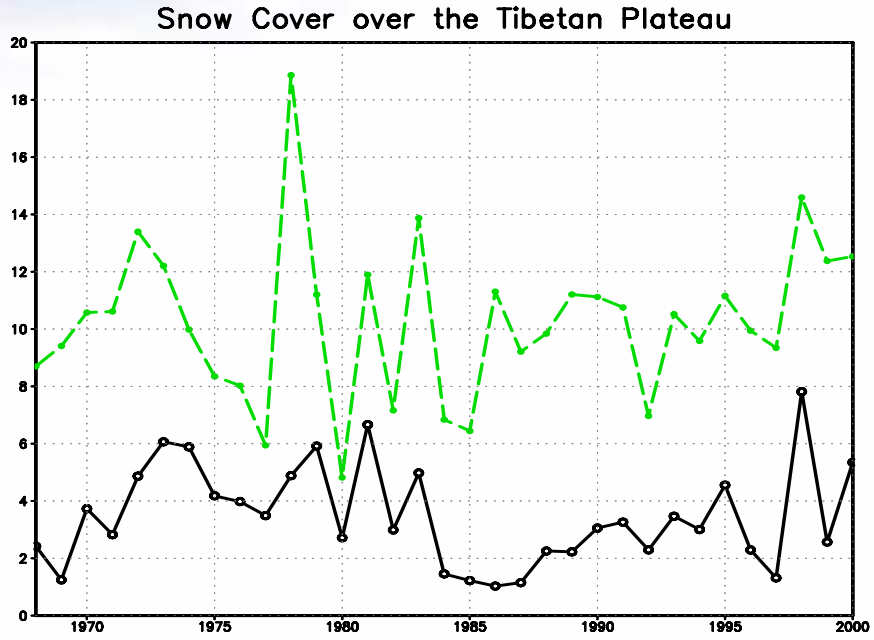

(b)

Figure 15 Time-series of the snow cover derived from SSM/I satellite data (a) and the AVHR (b). For (a), the bold (thin) line indicates winter (spring) snow cover. For (b), the solid (dashed) line denote spring (winter) condition. These data are provided by Dr.D.A.Robinson.

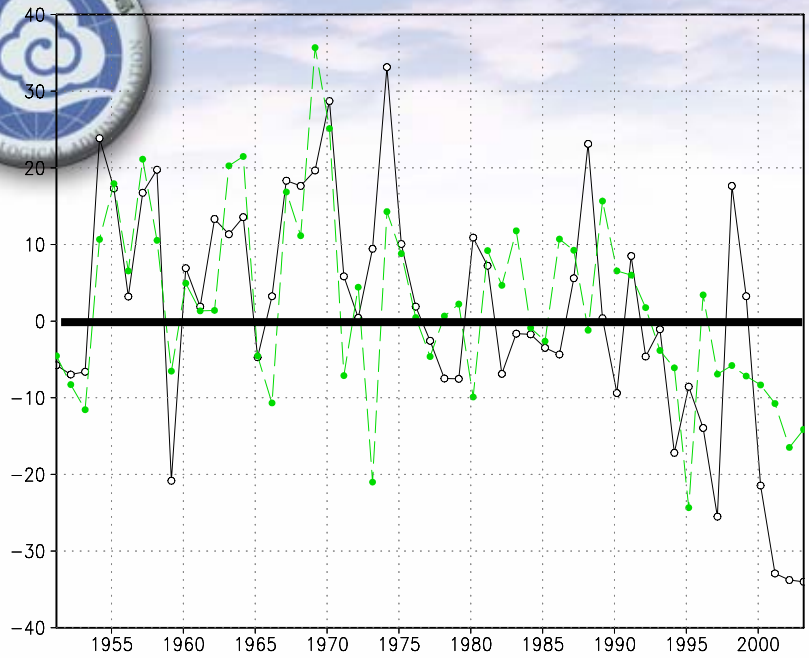

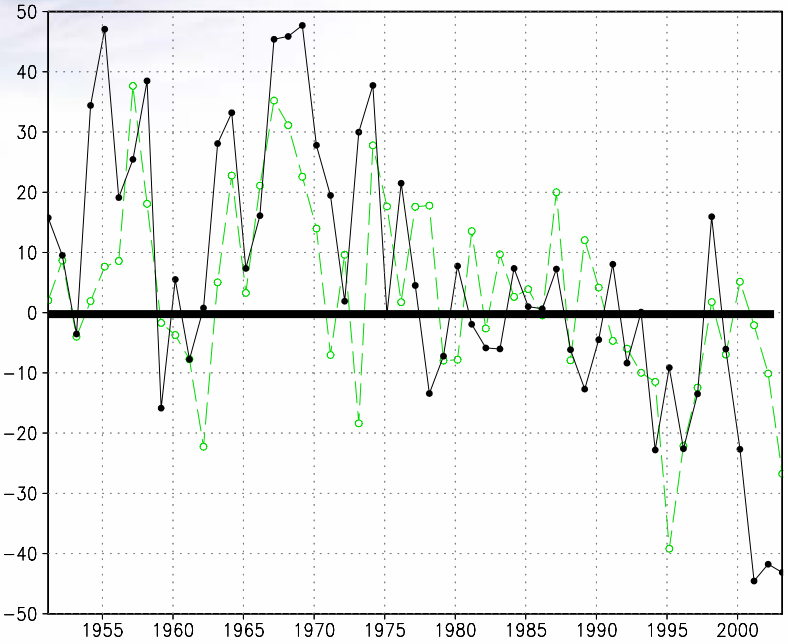

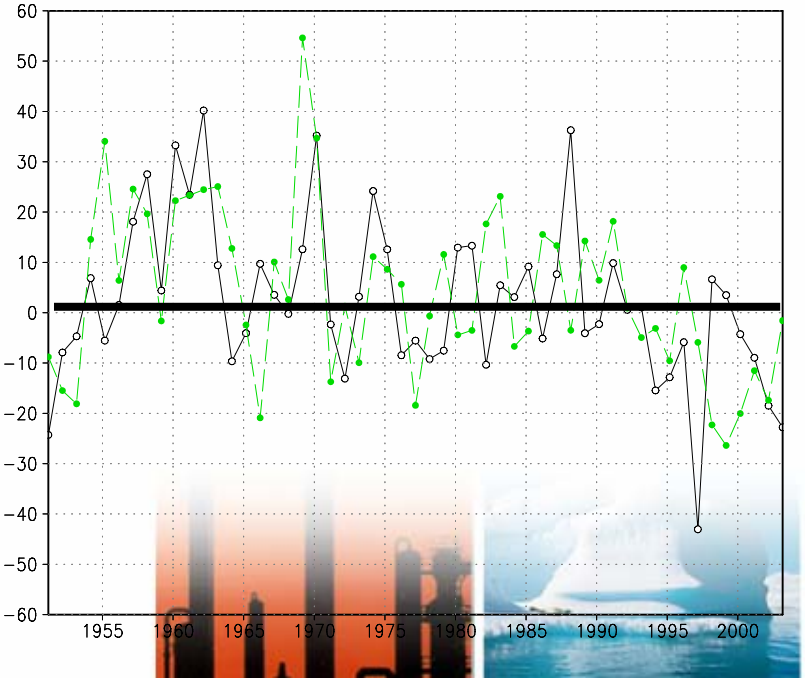

Figure 16 Time series of the anomalous vertically integrated (surface 100hPa) apparent heat source (Q1) averaged for all Tibetan Plateau (75～105° E，27.5~42.5° N)(a), the eastern Tibetan Plateau (92.5～105° E，27.5~50° N) (b) and the western Tibetan Plateau (75～92.5° E，30~37.5° N) (c). Solid (dashed) lines denote summer (spring) curves. Unit: Wm^{-2}

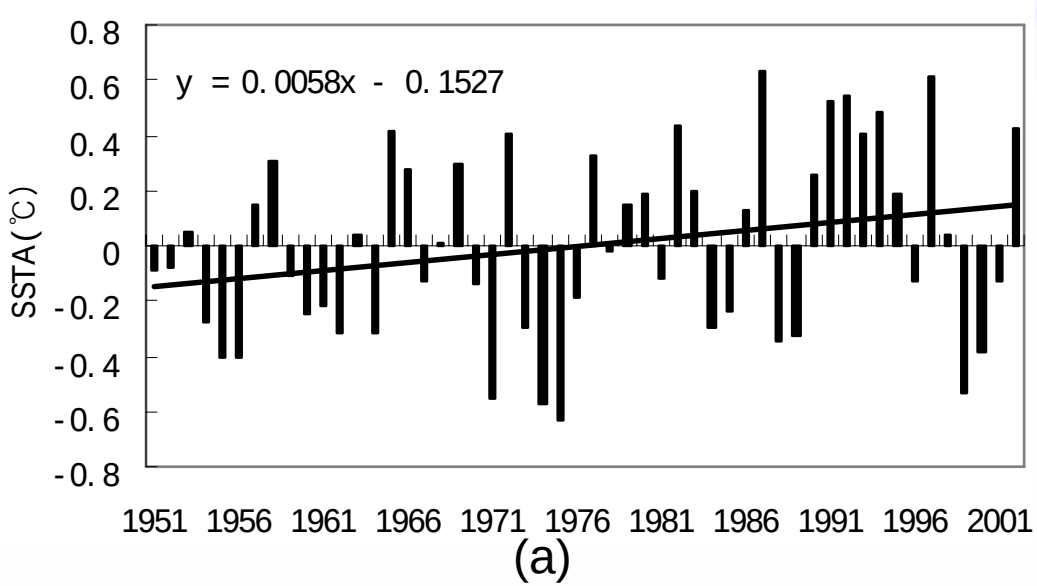

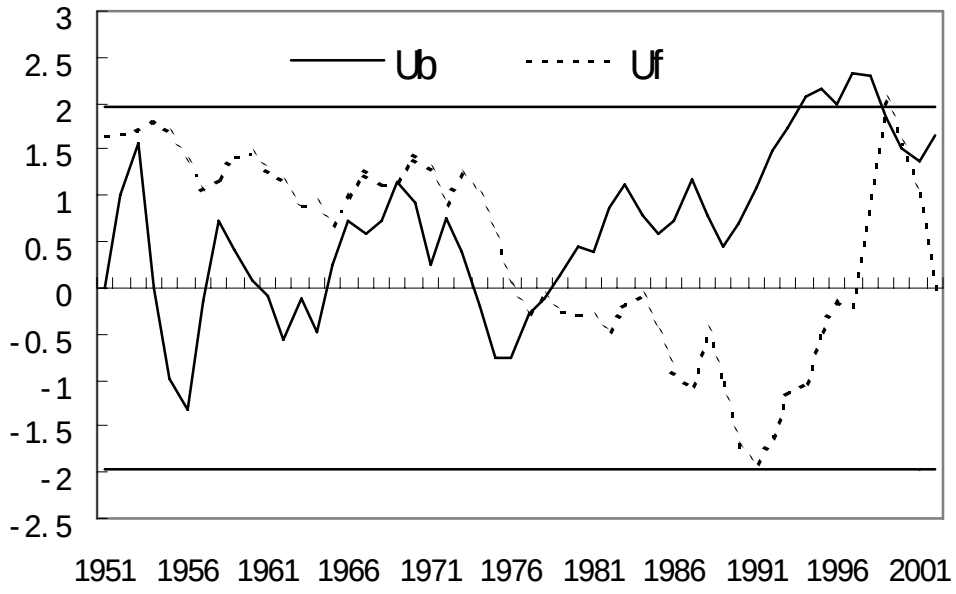

Figure 17 (a) Time-series of annual mean SST departures over the equatorial central Pacific (140° E～140° W，5° S～5° N). Solid line is the linear trend. (b) The M-K test of above annual mean SST time series. Horizontal bars are critical values with statistical significance of α =0.05





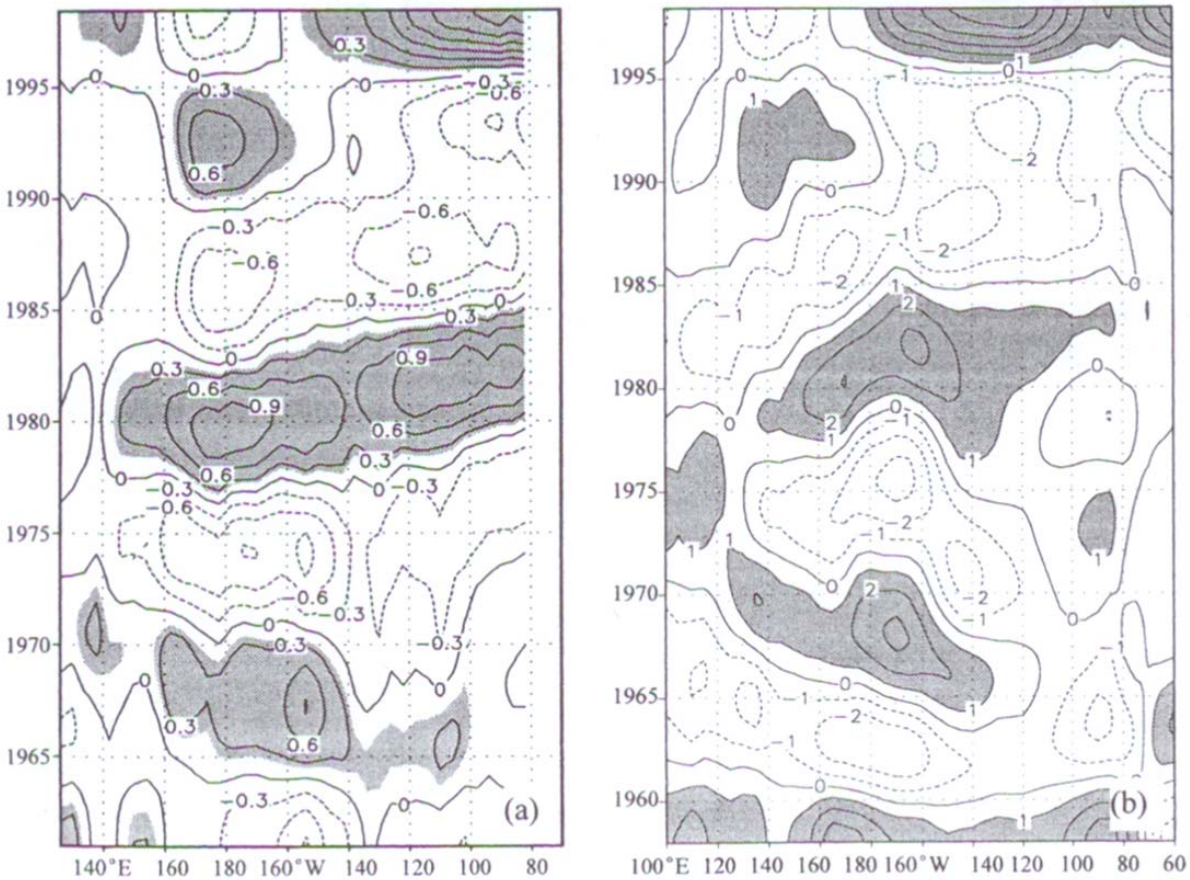

Figure 18 Longitude-time cross-sections of SSTA decadal component (a) (Unit: ℃) and 850hPa zonal wind (b) (Unit: ms-1) (Zhang, Ding, Yi, 2002)

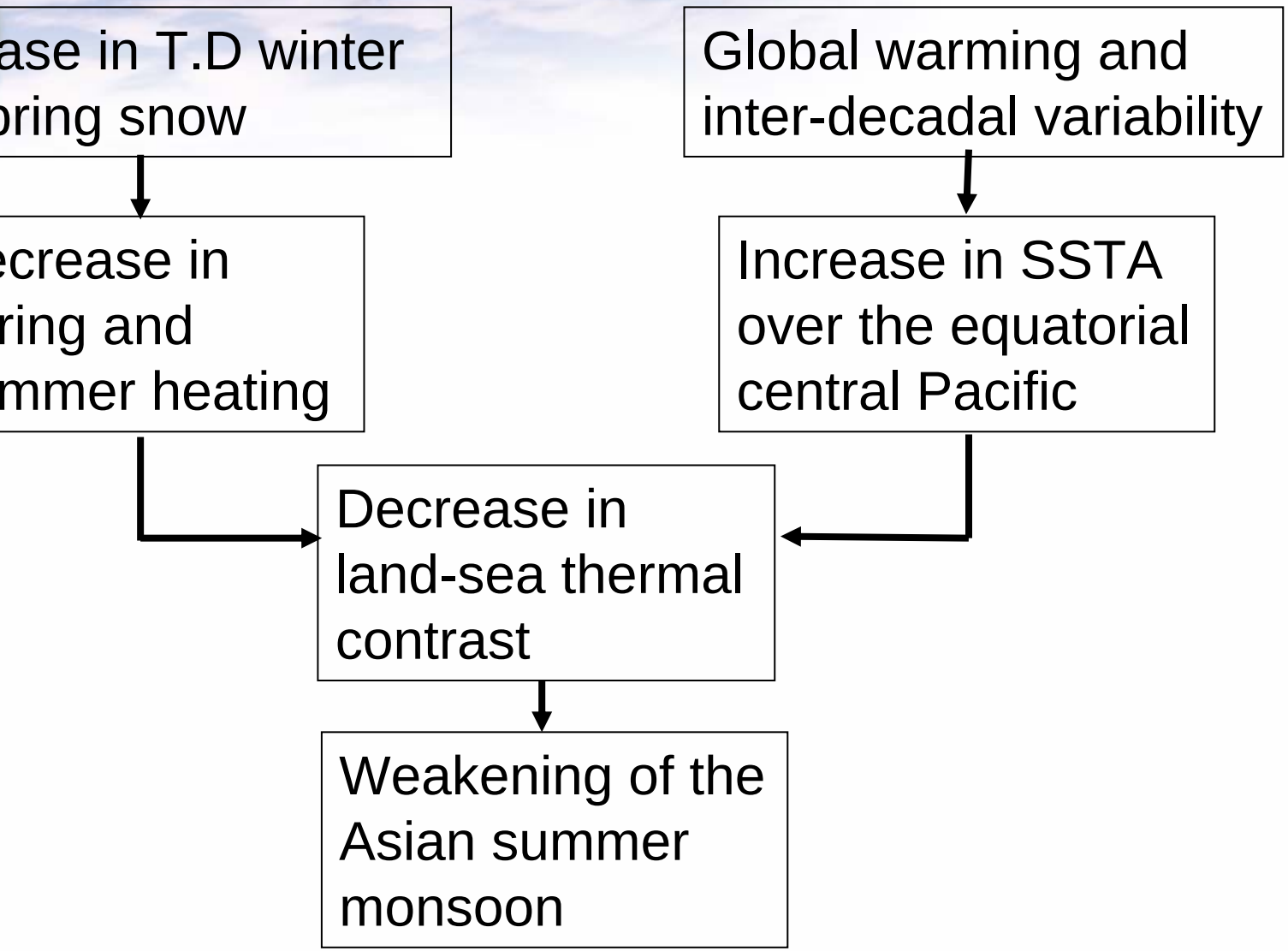

Figure 19 Possible cause of weakening of the Asian summer monsoon

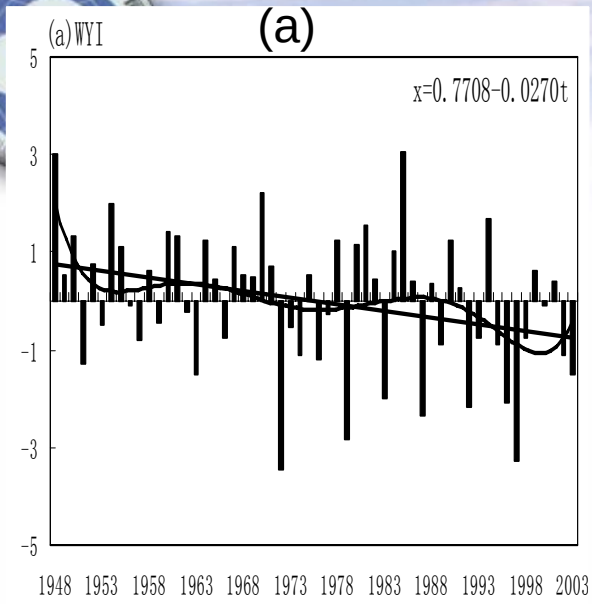

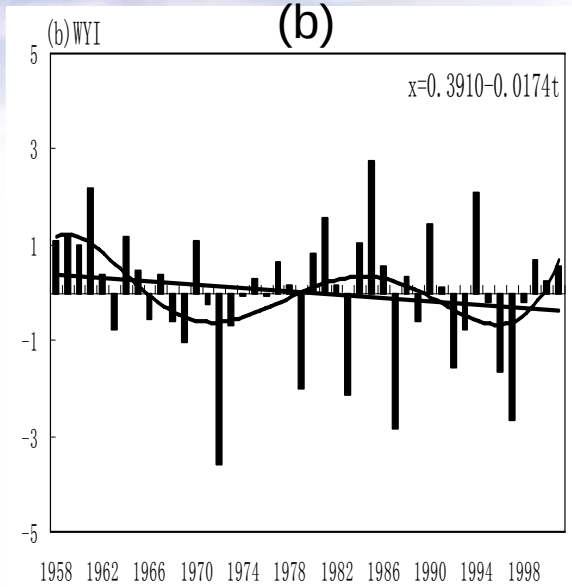

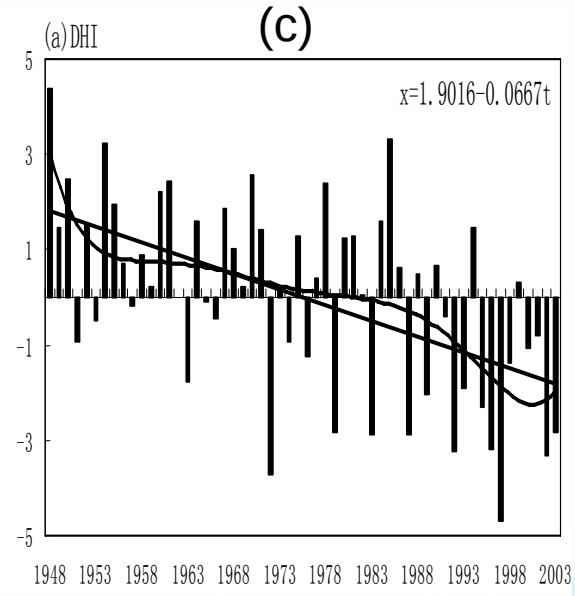

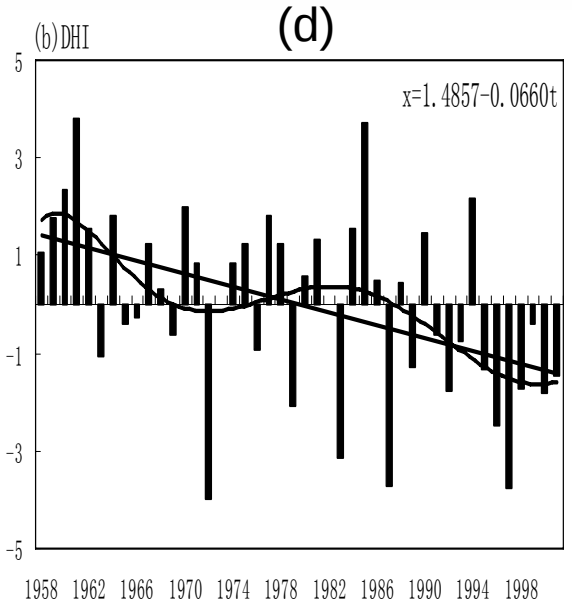

Figure 20 Time-series of anomalous summer monsoon indices for WYI estimated by using NCEP Reanalysis dataset (a) and using ERA-40 Reanalysis dataset (b); and DHI estimated by using NCEP Reanalysis dataset (c) and using ERA-40 Reanalysis dataset (d). WYI=U_{850}-U_{200}. DYI=U_{850}-U_{150}. Bold straight line denote the linear regression trend. The no smoothed curves are obtained with the 6-order polynomial fitling. Unit: *m/s*

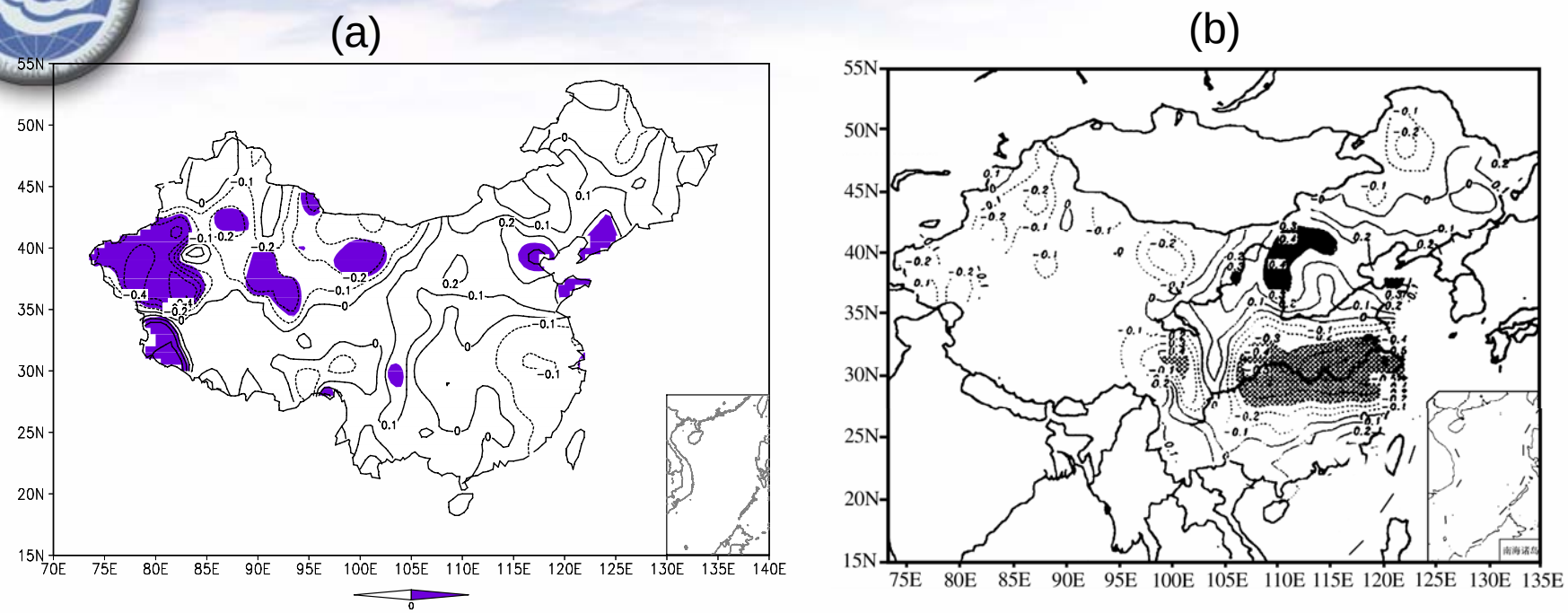

Figure 21 Correlation relationship of the Asian summer monsoon and precipitation in China: (a) simultaneous correlation between all India monsoon rainfall and Eat Asian rainfall in June-August. Shaded regions reach the confiden ficant level of 90%, and (b) correlation relationship between the East Asian summer monsoon index and summer rainfall in China (Taken from Sun et al., 2001). Positive correlation coefficients are indicated by solid lines (dashed) lines.

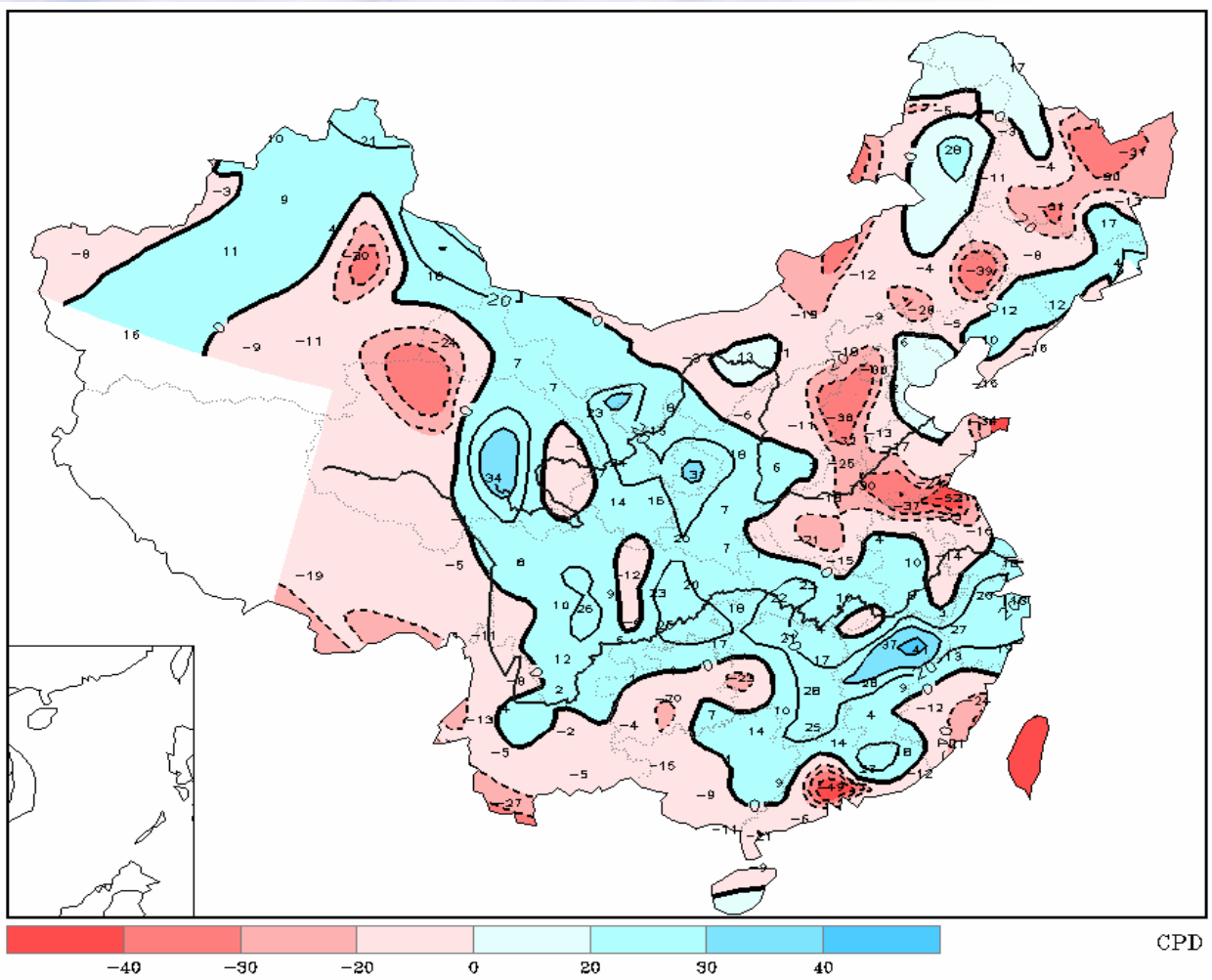

Figure 22 Correlation field between preceding winter and spring snow days over the Tibetan Plateau and subsequent summer precipitation in China. Solid (dashed) lines represent positive (negative) correlation coeffients (NCC, 1998)

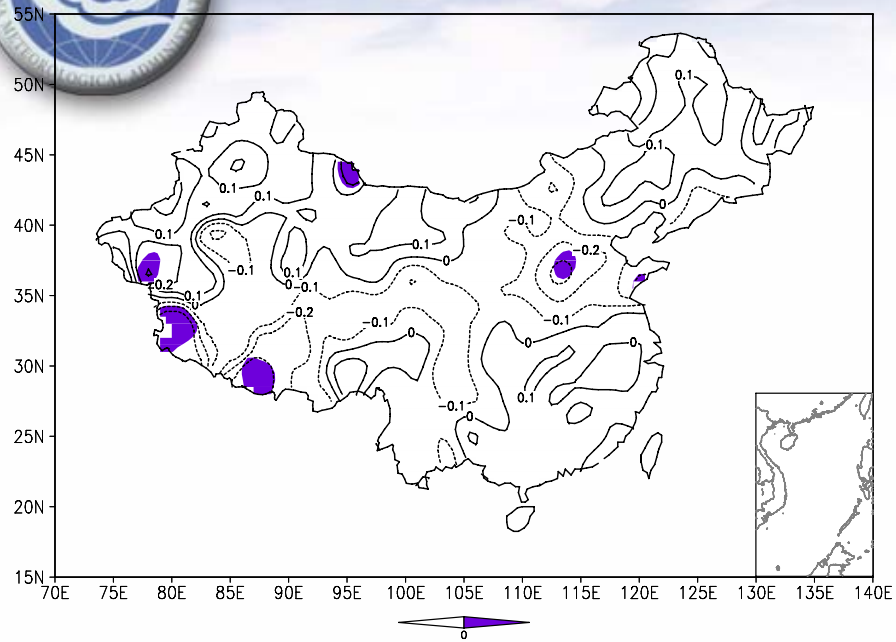

(a)

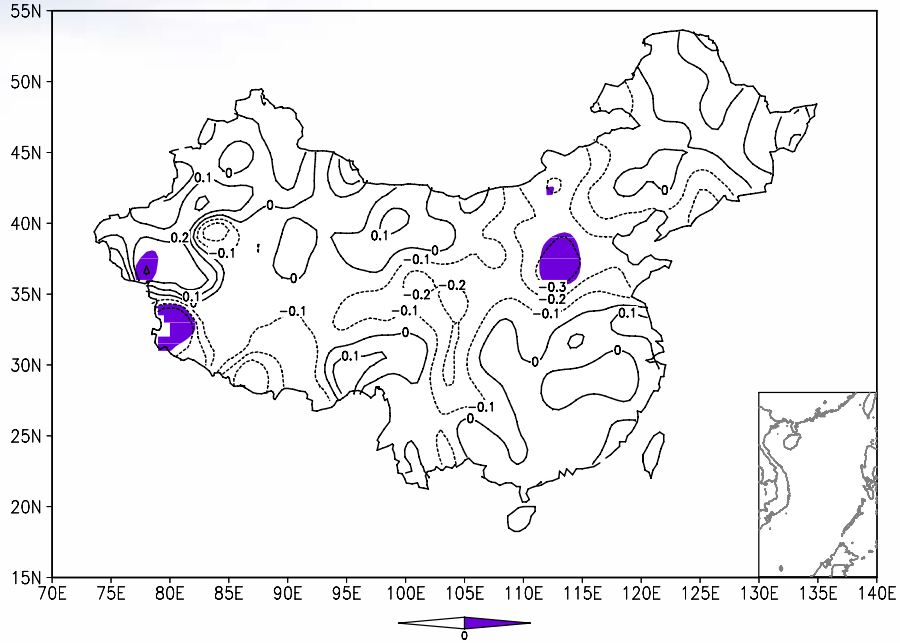

(b)

Figure 23 Correlation fields between annual mean SSTA in the equatorial central Pacific and the summer precipitation in China (a) and the summer SSTA and the summer precipitation in China

4. Projection of the next regime shift of the precipitation in China

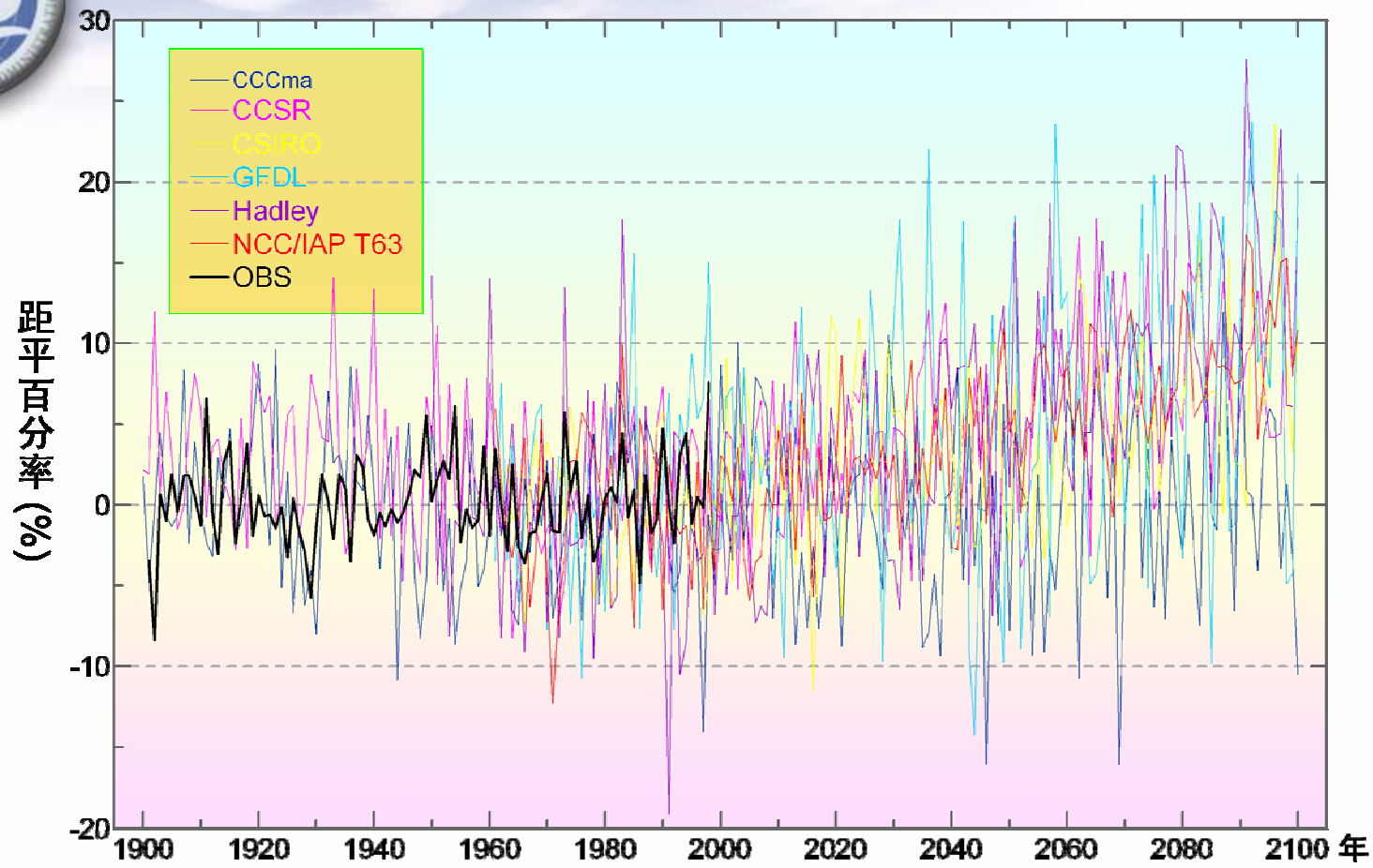

Figure 24 Simulation of precipitation in China for the past 100 years and projection for the next 100 years with consideration of different emission scenarios of CO_2 and sulfate aerosols by using NCC CGCM (NCC, 2004)

Figure 25 Time-series of precipitation departures in Northwest China (top), North China (middle) and all China (bottom) simulated for 1900-2000 and projected for 2001-2100 by using NCC CGCM (NCC,2004)

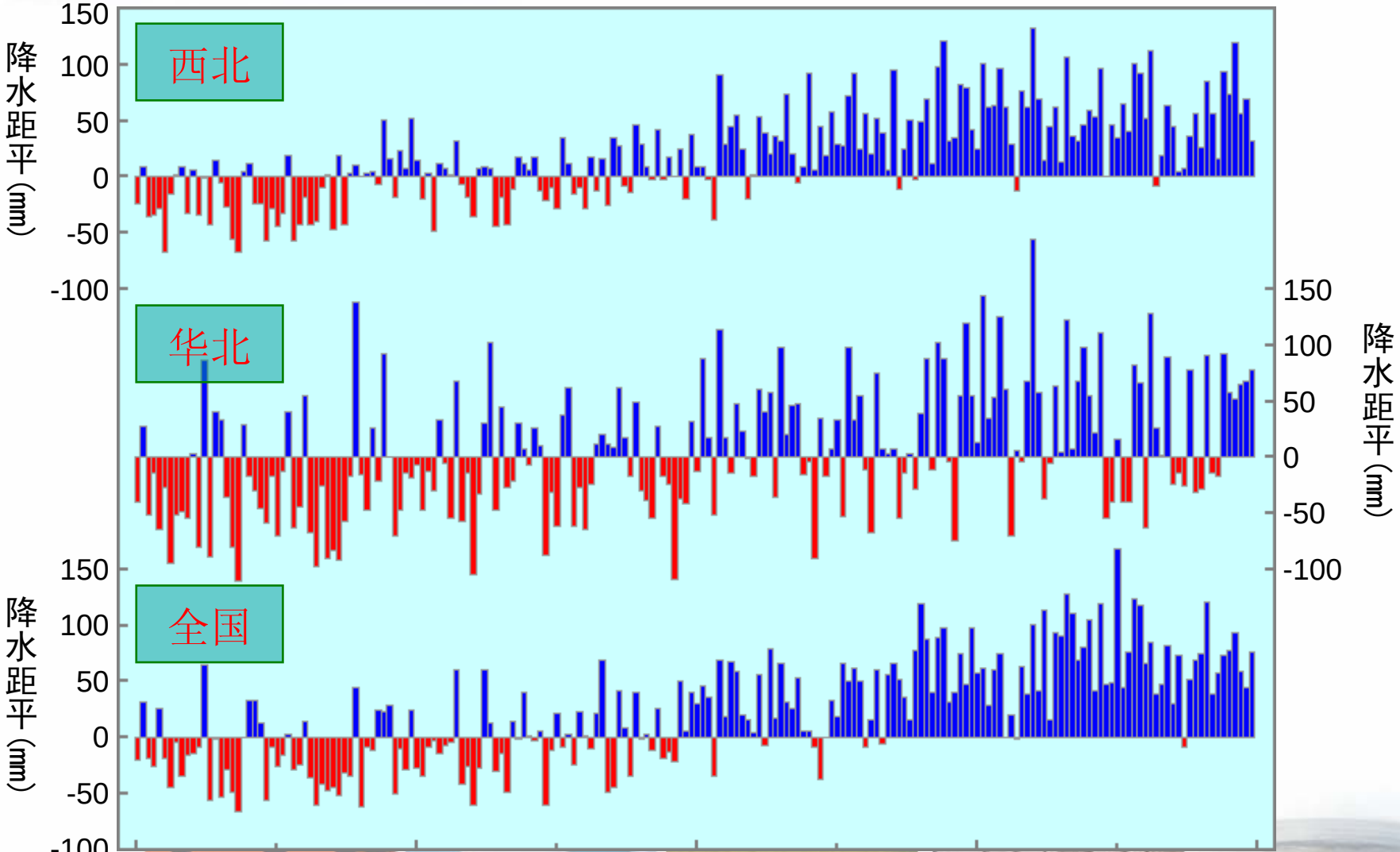

Thank you!